Hindawi
International Journal of Antennas and Propagation
Volume 2022, Article ID 5145743, 11 pages
https://doi.org/10.1155/2022/5145743

Research Article

A New Radar Echo Generation Model for Ultra-Low Altitude Targets in Far-Field Conditions

Zhao Long Wang, Chuang Ming Tong, Tong Wang, Yi Jin Wang, and Qing Kuan Wang

Air and Missile Defense College, Air Force Engineering University, Xi'an, China

Correspondence should be addressed to Zhao Long Wang; wangzhaolong2022@163.com

Received 4 June 2022; Revised 31 August 2022; Accepted 17 September 2022; Published 6 October 2022

Academic Editor: Hervé Aubert

This paper proposed a new radar echo simulation method for ultra-low altitude targets in far-field conditions. Based on the electromagnetic (EM) scattering calculation of target and environment, combined with the weighted four-path model, the scattering data of target, environment, and multipath are obtained. The Range-Doppler ring partitioning method is used to determine the size of the minimum resolution units, and then the environment is divided into several scattering elements. By using the method of temporal decomposition, the wide-time pulse is decomposed into a plurality of narrow pulse signals, and the narrow pulses act on scattering elements with different distances and orientations in space. The total echo is obtained by a linear superposition of the responses of each scattering unit. In addition, the numerical results with different parameters, including signal bandwidths, target types, and target height, are simulated and analysed. The simulation results demonstrate that the proposed method can provide a better description of the scattering characteristics of sea-skimming targets in complex scenes in far-field conditions. Meanwhile, it can be applied to the detection and recognition of ultra-low altitude targets above the sea surface.

1. Introduction

With the rapid development of radar observation of sea targets in military and civil fields, the research of electromagnetic (EM) scattering echo in the composite environment of the target sea surface has attracted more and more attention. Due to the interference from environmental clutter and multipath echo between target and sea, it is difficult for radar to detect ultra-low altitude sea-skimming targets accurately. At present, simply studying the EM scattering characteristics between the target and the environment cannot meet the needs of analyzing the radar characteristics in complex scenes. Therefore, based on the accurate EM model and taking into account the interaction between the target and the sea background, the simulation of the radar echo signal under the complex background has the advantage of being direct and clear and has become a hot spot for radar simulation research in recent years.

The echo signal obtained by radar is actually a signal transmission process. The echo signal received by the radar results from the convolution of scattering data and the transmitted signal. The traditional sea clutter simulation is usually obtained by fitting the measured sea clutter data [1]. Although it conforms to the statistical characteristics, it lacks the scattering mechanism and cannot reflect the relationship between the sea clutter and the transmitted signal. At the same time, when the target flies at ultra-low altitudes, it is difficult to obtain an accurate result due to the strong coupling between the target and the environment. A target radar echo is usually simulated based on the point scattering center and multiscattering center models. Their idea is to use the radar cross-section (RCS) of the scattering center to represent the overall scattering amplitude of the target. However, in the ultra-low altitude scene, the echo received by the radar includes target echo, clutter, and multipath echo. It is difficult to accurately describe the radar echo characteristics of ultra-low altitude targets through several

scattering centers. Based on the scattering mechanism, the application of theEM calculation to echo simulation has practical application value. In Reference [2, 3], the modeling and simulation of sea clutter are carried out by using the EM calculation method. This kind of method is mainly applied to the ocean Doppler [4, 5] and the original echo signal of synthetic aperture radar [6, 7]. Reference [8, 9] studied the radar echo of a target on a dynamic sea surface. The above studies have completed the echo simulation analysis based on the EM calculation method. However, on the one hand, due to the limitation of the computational efficiency of the EM model, it is difficult to simulate the echo of targets above a large-area sea surface. On the other hand, the radar scene parameters are not considered in the actual detection process of ultra-low altitude targets. From the current research, the simulation of a radar echo for complex scenes is obviously insufficient.

To better analyze the radar echo in a complex scene, this paper proposes a new radar echo simulation method for ultra-low altitude targets in far-field conditions. Based on the EM scattering calculation of target and environment, combined with the weighted four-path model, the scattering data of target, environment, and multipath are obtained. The scattering results present the original echo, and the echo is processed by the signal processing. The innovation of this paper is to combine complex EM calculations with echo simulation. The simulation results demonstrate that the proposed method can provide a better description of the scattering characteristics of sea-skimming targets in complex scenes. Meanwhile, it can be applied to the detection and recognition of ultra-low altitude targets above the sea surface.

2. The Modified Four-Path Model

The scattering characteristics of ultra-low altitude sea-skimming targets are complex and variable; the radar echo basically contains target echo, sea clutter, and multipath echo between target and sea. The four-path model is an efficient way to describe the composite scattering mechanisms. However, the antenna beam of the radar seeker has a certain width, and the multipath interference entering from the main lobe or side lobe of the antenna will affect the detection ability of the radar seeker. In this paper, we adopt the Gaussian pattern [10] to modify the traditional four-path model, and its main lobe function expression is as follows:

$$G_{MB}(\theta) = \exp\left(\frac{-2\ln 2\theta^2}{\theta_B^2}\right), |\theta| \le \mu,$$
$$\mu = \theta_B\sqrt{\frac{\ln g_3}{(-2\ln 2)}}, \tag{1}$$

where θ_B is the half-power lobe width of the antenna and μ is the azimuth angle value when the main lobe gain is equal to g_3. In the Gaussian antenna pattern, there are mainly two side lobes around the main lobe, which can be expressed as follows:

$$\theta_{B1} = 0.5\mu\sqrt{\frac{(-2\ln 2)}{\ln(g_3/g_1)}},$$
$$\theta_{B2} = 0.5\mu\sqrt{\frac{(-2\ln 2)}{\ln(g_3/g_2)}}. \tag{2}$$

In the simulation of this paper, $g_1 = 0.01$, $g_2 = 0.00316$, $g_3 = 0.001$. The peak values of the gain of the first side lobe and the second side lobe are $G_1 = 10\log_{10}g_1 = -20$dB and $G_2 = 10\log_{10}g_2 = -25$dB. The other side lobe gains are set to $G_r = 10\log_{10}g_3 = -30$dB. The half-power beam width is taken as 5°, and the antenna pattern is obtained as shown in Figure 1.

Based on the traditional four-path model, the antenna pattern is introduced to modify it. Also, the modified four-path model is shown in Figure 2.

In Figure 2, h_{seeker} represents the vertical height of the seeker from the sea surface; H_{target} represents the vertical height of the ultra-low altitude target; R represents the spatial distance between the seeker and the target; and D represents the horizontal distance between the seeker and the target. The various parameters shown in Figure 2 meet the following relationships:

$$\begin{cases} h_{\text{seeker}} = R\cos\theta_1 + H_{\text{target}} \\ D = R\sin\theta_1 \\ \theta_2 = \theta_3 = \tan^{-1}\left[\dfrac{D}{\left(H_{\text{target}} + h_{\text{seeker}}\right)}\right] \\ \theta_4 = \theta_1 \end{cases}. \tag{3}$$

Assuming that the main lobe of the seeker antenna is aligned with the target, the included angle between the multipath echo direction and the maximum gain direction of the main lobe is $\Delta\theta$, and $\Delta\theta = \theta_1 - \theta_2$. The maximum gain of the main lobe is $G_{MB}(\theta)|_{\theta=0^\circ} = 1$. Then, the correction coefficient of the antenna pattern can be expressed as follows:

$$\xi(\Delta\theta) = \frac{G(\Delta\theta)}{G_{MB}(\theta)\big|_{\theta=0^\circ}} = \begin{cases} G_{MB}(\Delta\theta), |\Delta\theta| \le \mu \\ G_{B1}(\Delta\theta), \mu \le |\Delta\theta| \le 2\mu \\ G_{B2}(\Delta\theta), 2\mu \le |\Delta\theta| \le 3\mu \end{cases}, \tag{4}$$

where $\mathbf{E}(\hat{\mathbf{k}}_i, \hat{\mathbf{k}}_s)$ and $\mathbf{E}'(\hat{\mathbf{k}}_i, \hat{\mathbf{k}}_s)$ represent the scattering fields from the target and the mirror target, respectively; $\hat{\mathbf{k}}_i$ and $\hat{\mathbf{k}}_s$ represent the unit vectors of the incident direction and scattering direction, respectively, and ρ represents the Fresnel reflection coefficient. In Figure 2, the four paths can be described as follows:

Path 1: Radar seeker-target-radar seeker. This path is the direct echo of the target, which is recorded as: $\mathbf{E}_1(\hat{\mathbf{k}}_{i1}, \hat{\mathbf{k}}_{s1})$.

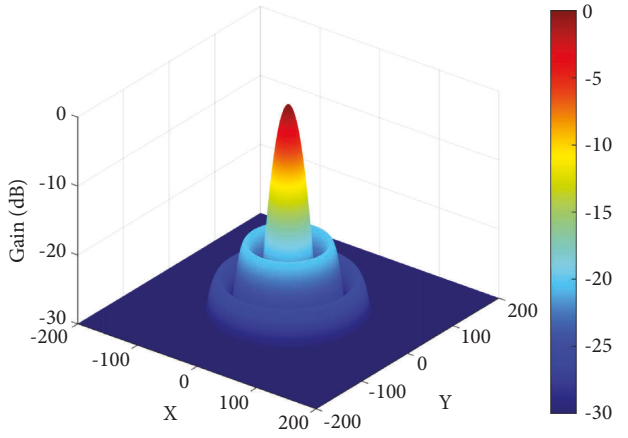

Figure 1: The schematic diagram of a Gaussian antenna pattern.

Path 2: Radar seeker-target-environment-radar seeker. The target echo on this path is reflected by the environment and is recorded as: $\rho \mathbf{E}_2'(\hat{\mathbf{k}}_{i2}, \hat{\mathbf{k}}_{s2})$.

Path 3: Radar seeker-environment-target-radar seeker. The EM wave on this path first passes through the reflection of the environment and then reaches the target. The echo is recorded as: $\rho \mathbf{E}_3(\hat{\mathbf{k}}_{i3}, \hat{\mathbf{k}}_{s3})$.

Path 4: Radar seeker-environment-target-environment-radar seeker. The EM wave on this path first passes through two reflections of the environment, and the echo is recorded as: $\rho^2 \mathbf{E}_4'(\hat{\mathbf{k}}_{i4}, \hat{\mathbf{k}}_{s4})$.

Finally, the four-path model based on modified antenna pattern can be expressed as follows:

$$\begin{aligned}\mathbf{E_s} &= \mathbf{E}_{\text{path1}} + \mathbf{E}_{\text{path2}} + \mathbf{E}_{\text{path3}} + \mathbf{E}_{\text{path4}} \\ &= \mathbf{E}_1\left(\hat{\mathbf{k}}_{i2}, \hat{\mathbf{k}}_{s2}\right) + \xi(\Delta\theta)\rho \mathbf{E}_2'\left(\hat{\mathbf{k}}_{i2}, \hat{\mathbf{k}}_{s2}\right) \\ &\quad + \xi(\Delta\theta)\rho \mathbf{E}_3\left(\hat{\mathbf{k}}_{i3}, \hat{\mathbf{k}}_{s3}\right) + \xi(\Delta\theta)^2 \rho^2 \mathbf{E}_4'\left(\hat{\mathbf{k}}_{i4}, \hat{\mathbf{k}}_{s4}\right).\end{aligned} \tag{5}$$

3. Target and Environment Electromagnetic Model

The physical optics (PO) method is easy-to-use and efficient, suitable for echo simulation with a large amount of calculation. In high frequencies, the scattering of the target mainly comes from surface scattering and edge diffraction. The PO method is used to calculate the surface scattering of the target, and the method of equivalent current (MEC) is used to calculate the edge diffraction of the target. According to the PO method [11], the far-field scattering of the target can be expressed as follows:

$$\mathbf{E}^s \approx \frac{jk_0}{4\pi} \frac{e^{-jk_0 r}}{r} \left[\hat{\mathbf{s}} \times \left(\mathbf{M}_s + \eta_0 \hat{\mathbf{s}} \times \mathbf{J}_s\right)\right] \cdot \Delta A \cdot I, \tag{6}$$

where $\mathbf{J}_s$ and $\mathbf{M}_s$ represent the electric and magnetic current on the surface, ΔA is the area of the triangular facet. I is the electric current, j represents the imaginary unit, k_0 represents the EM wave number in free space, η_0 represents the wave impedance er in free space, r represents the modulus of the field position vector.

When calculating the far-field scattering of an ultra-low altitude target, the edge structure contained in the target model must also be fully considered. Based on MEC [12], the edge diffraction field is obtained by substituting the equivalent electric and magnetic currents into the radiation equation, as shown in

$$\mathbf{E}^{\mathbf{d}} = \frac{jk_0}{4\pi} \frac{e^{-jk_0 r}}{r} \int_C \left\{\eta_0 \hat{\mathbf{s}} \times \left[\hat{\mathbf{s}} \times \mathbf{J}(\vec{r}\,')\right] + \hat{\mathbf{s}} \times \mathbf{M}(\mathbf{r}')\right\} e^{-jk_0 \hat{\mathbf{s}} \cdot \mathbf{r}'} \mathrm{d}l, \tag{7}$$

where $\mathbf{J}(\mathbf{r}')$ and $\mathbf{M}(\mathbf{r}')$ represent the equivalent edge of electric and magnetic current. r represents the modulus of the field point position vector in the far field. $\hat{\mathbf{s}}$ is the unit vector of the direction of observation. $\mathbf{r}'$ is a radial vector from the origin to a point on the edge. dl is the arc length increment along edge C.

The two-scale model (TSM) is mainly used in the scattering calculation of rough surfaces with a large spatial scale range. This method has the advantage of not relying on the size of a large contour panel, which is convenient for the flexible division of scattering units in radar echo modeling. As shown in Figure 3, the environment surface contains the spatial spectrum distribution of high and low frequency. The low-frequency part corresponds to the large-scale contour distribution, and the Kirchhoff approximation (KA) method is used for its calculation. The high-frequency part corresponds to the small-scale local contour of the sea surface, and the EM scattering coefficient is calculated by the Small Perturbation method (SPM). At the same time, the small-scale part is modulated by the inclination of the large-scale part, and the total scattering cross section can be considered as the combination of the two parts.

The two-scale model can be expressed as [13, 14]:

$$\begin{aligned}\sigma_{\alpha\beta} &= \sigma_{\alpha\beta}^{KA} + \langle \sigma_{\alpha\beta}^{SPM} \rangle \\ &= \frac{\pi k_0^2 |\mathbf{q}|^2}{q_z^4} \left| U_{\alpha\beta}^{KA} \right|^2 P\left(z_x, z_y\right) + \int_{-\infty}^{\infty} \int_{-\cot\theta_i}^{\infty} \sigma_{\alpha\beta}^{SPM}(\theta_i') \left(1 + z_x \tan\theta_i\right) P\left(z_x, z_y\right) dz_x dz_y,\end{aligned} \tag{8}$$

where $\mathbf{q} = k_0(\hat{k}_s - \hat{k}_i)$. $P(z_x, z_y)$ is the joint probability density function of the slope of the rough surface. U^{KA} is a factor related to the reflection coefficient and polarization [15]. θ_i and θ_i' are the global and local incidence angles,

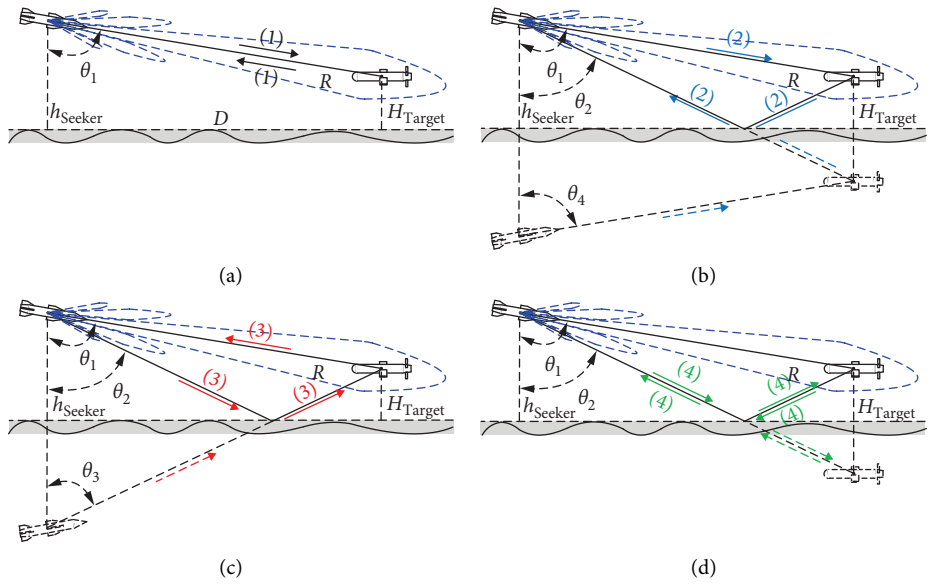

Figure 2: The schematic diagram of the modified four-path model. (a) Path1. (b) Path 2. (c) Path3. (d) Path4.

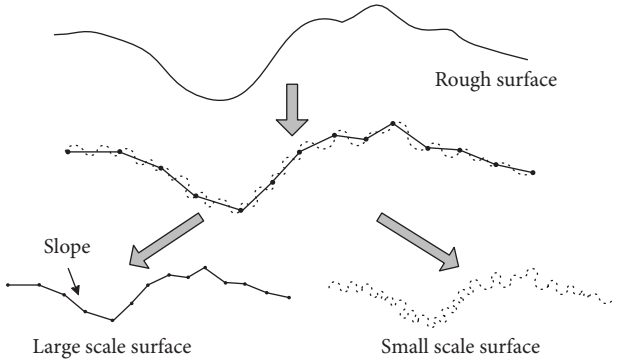

Figure 3: The schematic diagram of the two-scale model.

respectively. $\sigma_{\alpha\beta}^{SPM}(\theta_i')$ is the backscattering coefficient of the panel in the local coordinate system [16].

4. Electromagnetic Model Verification

To verify the correctness and effectiveness of the PO + MEC algorithm, its calculation results are compared with those of the multilevel fast multipole algorithm (MLFMA) based on the accurate numerical algorithm. The operating frequency of the radar is 15 G Hz in the Ku band. The calculation object is a missile-like target with a length of 5.56 m. The missile head faces the x-direction and is placed along the x-axis. The incident angle is set as follows: $\theta_i = -90^\circ \sim 90^\circ$, $\varphi_i = 0^\circ$. The monostatic scattering RCS of the two algorithms under vertical-to-vertical (VV) polarization is shown in Figure 4.

As shown in Figure 4, the PO + MEC algorithm can well reflect the scattering of triangular facets and edges of the target. The simulation results can obtain accurate solutions compared with the MLFMA. At the same time, the computing time of PO + MEC is 386 s, and the computing time of MLFMA is 1654 s. From the comparison results of the two

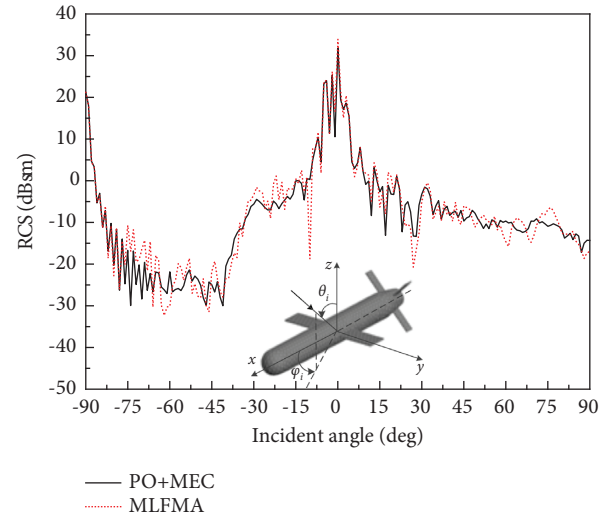

Figure 4: The schematic diagram of two-scale model.

algorithms, the PO + MEC method, on the basis of ensuring the calculation accuracy, it can effectively save the calculation time, which is applicable to the calculation of target echo in this paper.

To illustrate the rationality of the TSM algorithm, the scattering results of the Elfouhaily sea surface [17] are simulated and compared with the measured experimental data of the flume in reference [18]. The size of the sea surface is 200 m ∗ 200 m. The dielectric constant is (46–j36), taken as the value when the seawater temperature is 20°C, and the salinity is 35‰. The wind speed at 10 m above the sea surface is 5 m/s. The radar operating frequency is 15 G Hz in the Ku band. The normalized backscattering results are shown in Figure 5.

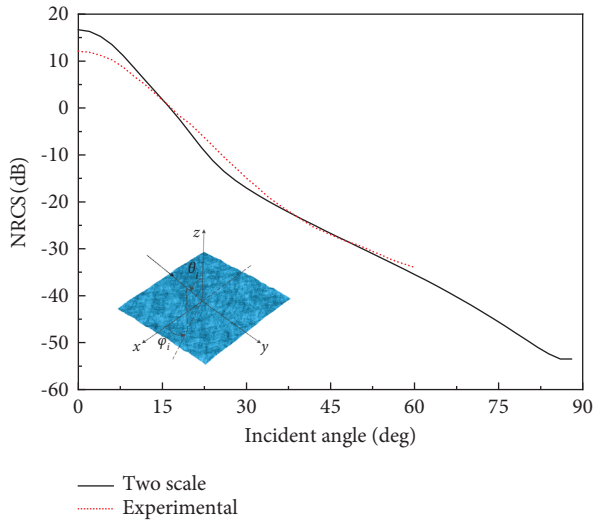

FIGURE 5: The normalized backscattering results of the two methods.

5. Radar Echo Signal Model

5.1. Space Decomposition Method. In the range of radar antenna illumination, the clutter area cannot be simply considered as a single scatterer. Therefore, the scattering area is divided into several scattering elements using the Range-Doppler ring partitioning method [19]. The antenna gain, Doppler frequency shift, distance, incidence angle, and clutter scattering rate of each element are constant. As shown in Figure 6, the environment is divided into multiple units within the radar-illuminated area.

ΔR is the width of the distance ring, which is determined by the distance resolution, which can be written as follows:

$$\Delta R = \frac{c}{2B_W}, \tag{9}$$

where c is the propagation speed of the EM wave and B_W is the frequency modulation bandwidth. $\Delta\varphi$ is the azimuth interval, which is related to the Doppler resolution, which can be written as follows:

$$\Delta\varphi \approx \frac{\lambda f_r}{4Kv_R \cos\varphi}, \tag{10}$$

where f_r is the pulse repetition frequency, K is the number of pulses in a coherent processing interval (CPI), v_R is the seeker speed, and φ is the pitch angle of a certain Range-Doppler unit. The area of the unit is set as A_c, and the RCS of the clutter scattering unit can be written as follows:

$$\sigma_c = \sigma_{\alpha\beta} A_c. \tag{11}$$

5.2. Temporal Decomposition Method. Pulse radar is adopted, and the transmitted signal s_t is expressed as follows:

$$s_t(t) = u(t) \exp\left[\mathrm{j}2\pi\left(f_0 t + \frac{Kt^2}{2}\right)\right], \tag{12}$$

where f_0 is the carrier signal frequency, $K = B/T_p$ is the linear frequency modulation frequency, B is the linear frequency modulation signal bandwidth, and $u(t)$ is the rectangular modulation pulse.

In the process of detecting targets, the radar transmits a wide-time pulse-linear frequency signal. A single pulse contains multiple pulse resolution units. Using the method of temporal decomposition, the wide pulse is decomposed into a plurality of narrow pulse signals, and the narrow pulses act on scattering elements with different distances and orientations in space. The decomposed emission signal can be expressed as follows:

$$s_t(t) = \sum_{i=0}^{N_b-1} \exp\left[\mathrm{j}2\pi\left(f_0 t + \frac{Kt^2}{2}\right)\right] \mathrm{rect}\left(\frac{t - i\tau_p}{\tau_p}\right) \quad 0 \le t \le T_p, \tag{13}$$

where τ_p is the width of a narrow pulse, and N_b is the number of narrow pulses. rect$[\cdot]$ is the envelope of the rectangular pulse.

The echo response of each scattering unit on the narrow pulse is calculated, and the total echo is obtained by linear superposition of the responses of each scattering unit, as shown in Figure 7.

The target is divided into several triangular facets, and the environment is composed of a series of Range-Doppler units. The total echo signal is equal to the vector superposition of the echo signals of each small unit, and the echo of each small unit can be regarded as the echo of its center point. For monostatic radar, the radar echo at a certain time t can be expressed as follows:

$$s_r(t) = \sqrt{\frac{\lambda^2}{(4\pi)^3 R^4 L}} G\gamma s_t(t-\tau) \exp\left[\mathrm{j}2\pi f_d (t-\tau)\right], \tag{14}$$

where R represents the distance between the seeker and the target. L represents the amplitude attenuation factor. G is the radar antenna gain. γ is the Radar complex scattering cross-section, which can be expressed as $\gamma = \sqrt{\sigma}\exp(\mathrm{j}\phi)$. f_d is the Doppler shift.

$$s_r(t) = A\mathrm{rect}\left(\frac{t - 2R/\mathrm{c}}{T_p}\right)\varphi\left[t - \frac{2R}{\mathrm{c}}\right]\exp\left(-\mathrm{j}\frac{4\pi R}{\lambda}\right)\exp(\mathrm{j}2\pi f_d t). \tag{15}$$

In Equation (8) the signal is processed with zero intermediate frequency (zero-IF), and the zero-IF signal is obtained as follows:

$$s_r(k,t) = A(k)\mathrm{rect}\left[\frac{t - 2R(k)/\mathrm{c}}{T_p}\right]\varphi\left[t - \frac{2R(k)}{\mathrm{c}}\right]\exp\left[-\mathrm{j}\frac{4\pi R(k)}{\lambda}\right], \tag{16}$$

where $\varphi(t) = \exp(\mathrm{j}\pi K t^2)$ and A represent the reflectivity of each scattering point. (15) represents a single pulse echo from a point target that moves relatively slow. For a high-speed moving target, the echo from the kth unit after zero-IF processing can be expressed as follows:

The target speed information is contained in the change of $R(k)$. The target and environment are composed of N units, and the total echo is expressed as follows:

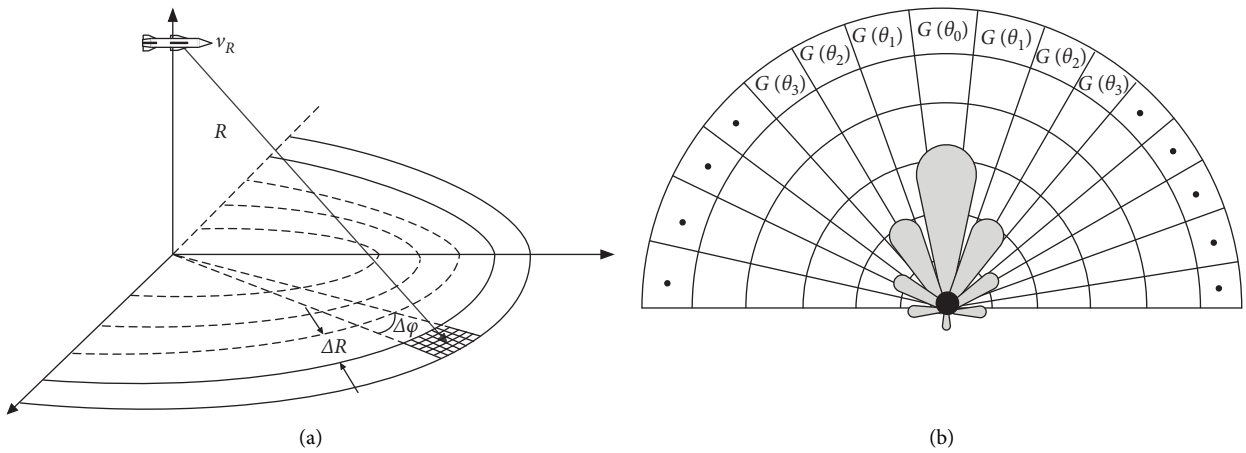

Figure 6: (a) Diagram of the Range-Doppler ring partition method; (b) top view.

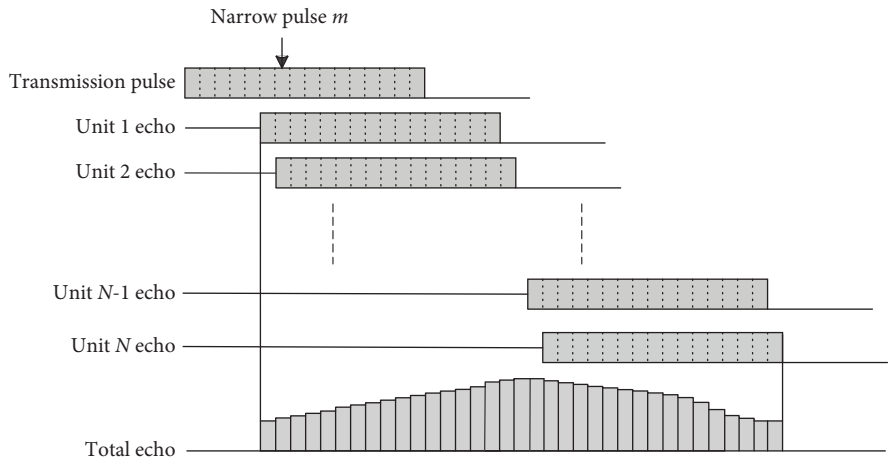

Figure 7: Diagram of the temporal decomposition method.

$$s_r(k,t) = \sum_{i=1}^{N} A_i(k)\mathrm{rect}\left[\frac{t - 2R_i(k)/\mathrm{c}}{T_p}\right]\varphi\left[t - \frac{2R_i(k)}{\mathrm{c}}\right]\exp\left[-\mathrm{j}\frac{4\pi R_i(k)}{\lambda}\right]. \quad (17)$$

Figure 8 shows the location relationship of target, environment, and radar. The radar position vector is Sp (1000 m, 0 m, 250 m), and its velocity vector is Vs (−500 m/s, 0 m/s, 0 m/s). The target position vector is Tp (0 m, 0 m, 50 m); its velocity vector Vt is (300 m/s, 0 m/s, 0 m/s).

Figure 9 shows the echo signal modeling process. The detection radar adopts the active system, and the peak values of the gains of the first side lobe and the second side lobe are $G_1 = -20$ dBand $G_2 - 25$ dB. The other side lobe gains are set to $G_r = -30$ dB. The half-power beamwidth is taken as 5°. The operating frequency is 15 G Hz in the Ku band, the number of accumulated pulses is 512, and the frequency modulation bandwidth is 60 M Hz. The antenna beam points to the center of the target, and both the incidence and receiving antennas are vertically polarized. The target model is a missile-like target with a length of 5.56 m. The wind speed at 10 m above the sea surface is 5 m/s, and the relative dielectric constant of the environment is (46–j36). Unless otherwise specified, the parameters of the later examples remain unchanged. Figure 10 shows the two-dimensional Range-Doppler diagram of the total echo in this scene.

6. Numerical Analysis

This section discusses the influence of different bandwidths, target heights, and target types on the echo signal. The simulation results show that the clutter effect is strong and the signal bandwidth affects the total echo.

Example 1. This example is used to verify the effectiveness of the target echo model in this paper. The targets are a conductor metal ball with a diameter of 0.6 m, and its RCS can be calculated directly, $\sigma = \pi r^2 = 0.2827\ \mathrm{m}^2$, a point target with an RCS of $0.2827\ \mathrm{m}^2$, and a missile-like target with a length of 5.56 m, respectively. The Range-Doppler spectrum of different targets under different bandwidths is shown in Figure 11.

As shown in Figure 11, when the radar bandwidth is 5 M Hz, the range resolution is 30 m. Also, as the diameter of the conductor ball target is 0.6 m, it can be regarded as a

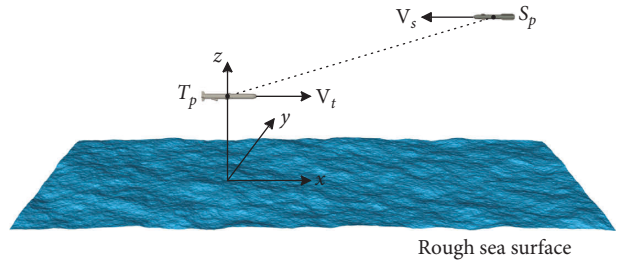

Figure 8: The schematic diagram of the target and environment models.

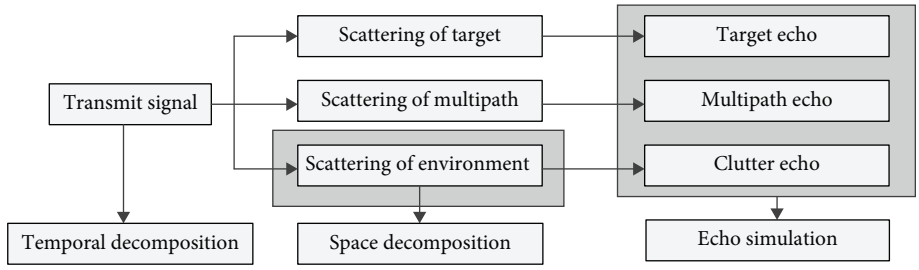

Figure 9: Diagram of the echo signal modeling process.

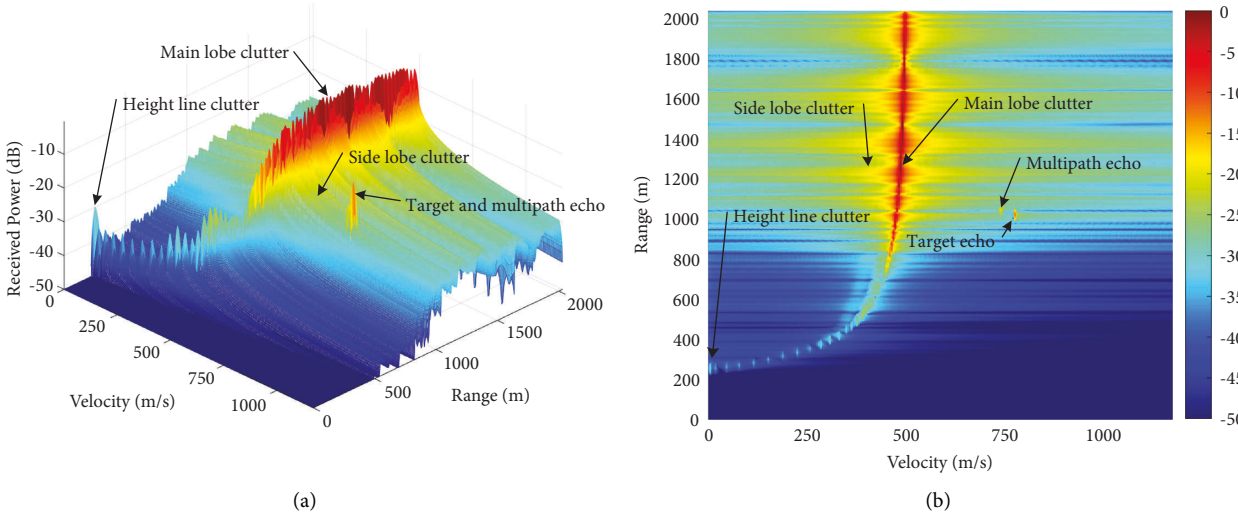

Figure 10: (a) The two-dimensional Range-Doppler diagram of the total echo; (b) top view.

point target. Figures 11(a) and 11(b) show that, under the same range gate, the echo of the conductor metal ball obtained by the EM calculation method is the same as that of the point target, which verifies the effectiveness of the target model. Figures 11(c) and 11(d) show the Range-Doppler spectrum of a missile-like target under different bandwidths. In the case of a narrow band, the target echo power is within the same range gate. When the bandwidth is increased to 60 M Hz, the range resolution is 1.5 m, the echo power of the target center is reduced, and the echo energy is dispersed in different range gates. At the same time, the target splits on the range gate, which shows that the echo model in this paper can show the Range-Doppler spectrum distribution of the extended target under different bandwidths.

Example 2. This example studies the effectiveness of multipath echo. Change the height of the target and the bandwidth of the transmitted signal, and other conditions remain unchanged. The Range-Doppler spectrum under different target heights and bandwidths is shown in Figure 12.

The multipath signal is generated by the coupling of environment and target, and its echo is similar to the target. When the target height is 50 m and 20 m, respectively, the path difference between the target and the mirror target is

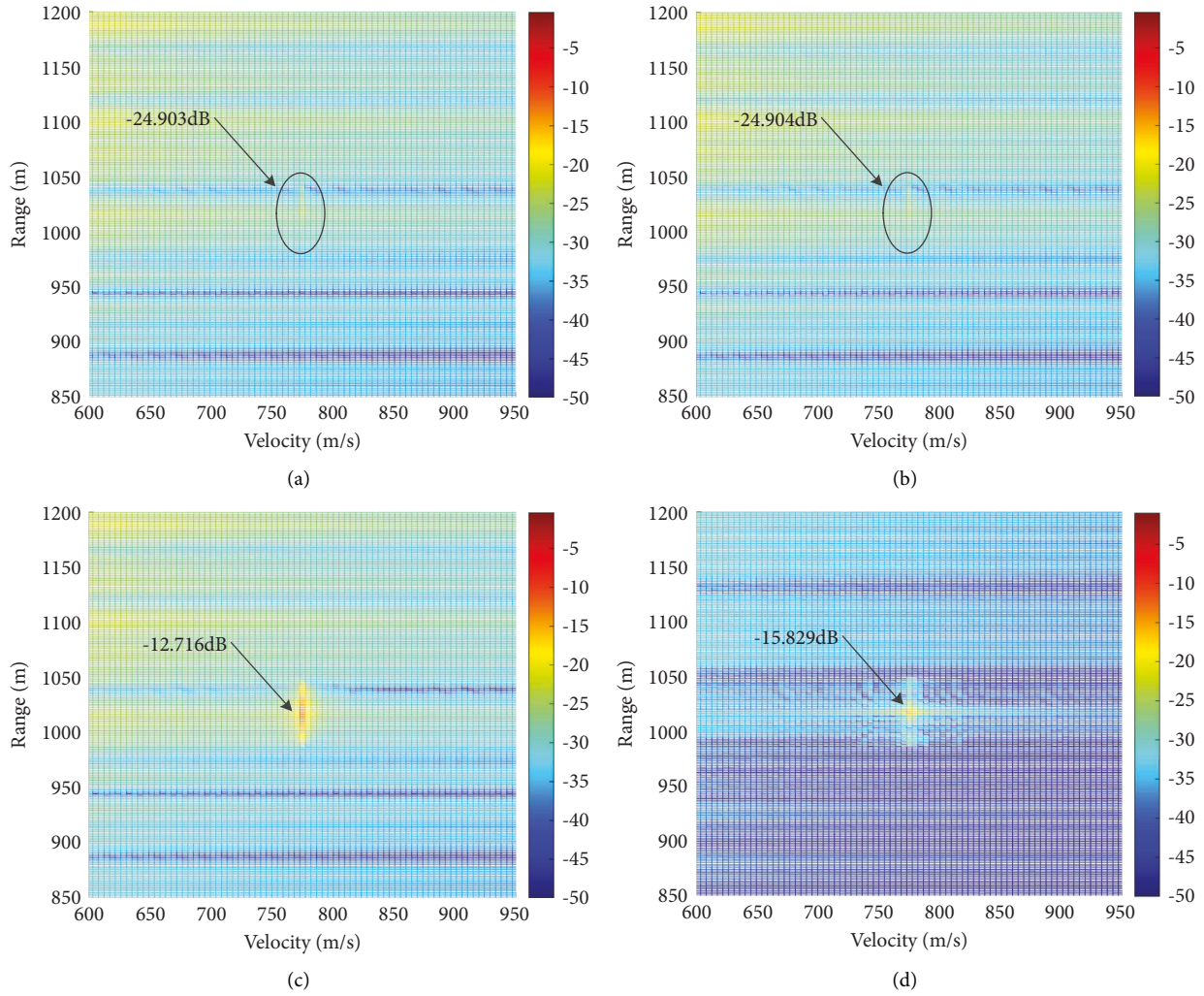

Figure 11: The Range-Doppler spectrum of different targets under different bandwidths. (a) Point target, $B = 5$ M Hz; (b) conductor metal ball, $B = 5$ M Hz; (c) missile-like target, $B = 5$ M Hz; (d) missile-like target, $B = 60$ M Hz.

24.2 m and 9.7 m, respectively. Comparing Figures 12(a) and 12(b), when the signal bandwidth is 10 M Hz, the radar range resolution is 15 m. As the target height decreases, the difference between multipath echo and target echo in range and velocity dimensions becomes smaller, making it difficult to distinguish between target and multipath echo in range dimensions. Comparing Figures 12(b) and 12(c), when the bandwidth of the signal is increased to 30 M Hz, the range resolution of the radar is changed to 5 m, so the multipath echo and target echo are dispersed in different range gates, and the target and multipath echo can be identified in the range dimension.

Example 3. This example studies the influence of bandwidth on clutter power. When the radial velocity between the target and the radar is zero or the RCS is small, the target echo will hide in the surrounding clutter. The amount of clutter in the unit is determined by the scattering coefficient and the resolution unit area. Increasing the signal bandwidth and reducing the resolution unit area can reduce the clutter power in the resolution unit and improve the signal-to-noise ratio (SNR). Figure 13 shows the echo power of target and clutter at different bandwidths.

As shown in Figure 13, the clutter power decreases significantly by increasing the signal bandwidth, while the target echo power changes slightly. Figure 14 shows the variation of SNR with the bandwidth change of a missile-like target with a length of 5.56 m in a single resolution unit. It should be noted that when the bandwidth increases and the target echo is dispersed into different range gates, the obtained SNR is the average of the SNR of all range gates.

As shown in Figure 14, when the bandwidth is less than 25 M Hz, the increase in SNR is obvious. When the bandwidth is greater than 25 M Hz, the change in SNR is small. The reason is that when the signal bandwidth is 25 M Hz, the range resolution is 6 m. When the range resolution is less than the target's projection on the range, although the clutter power of a single range unit decreases, the target echo power also disperses into multiple range gates, so the bandwidth has little impact on the SNR.

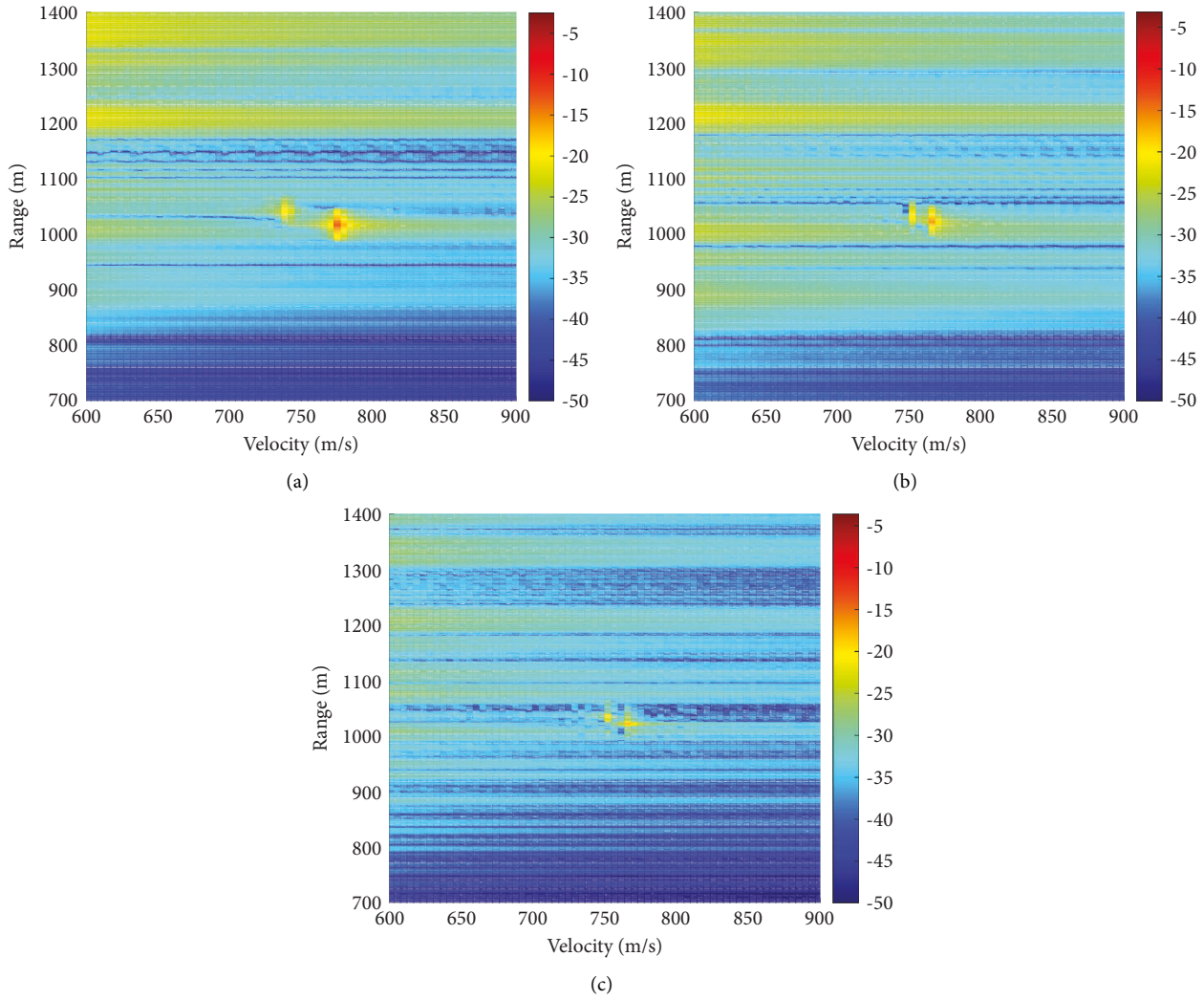

Figure 12: .The Range-Doppler spectrum under different target heights and different bandwidths (a) $H = 50$ M, $B = 10$ M Hz; (b) $H = 20$ M, $B = 10$ M Hz; (c) $H = 20$ M, $B = 30$ M Hz.

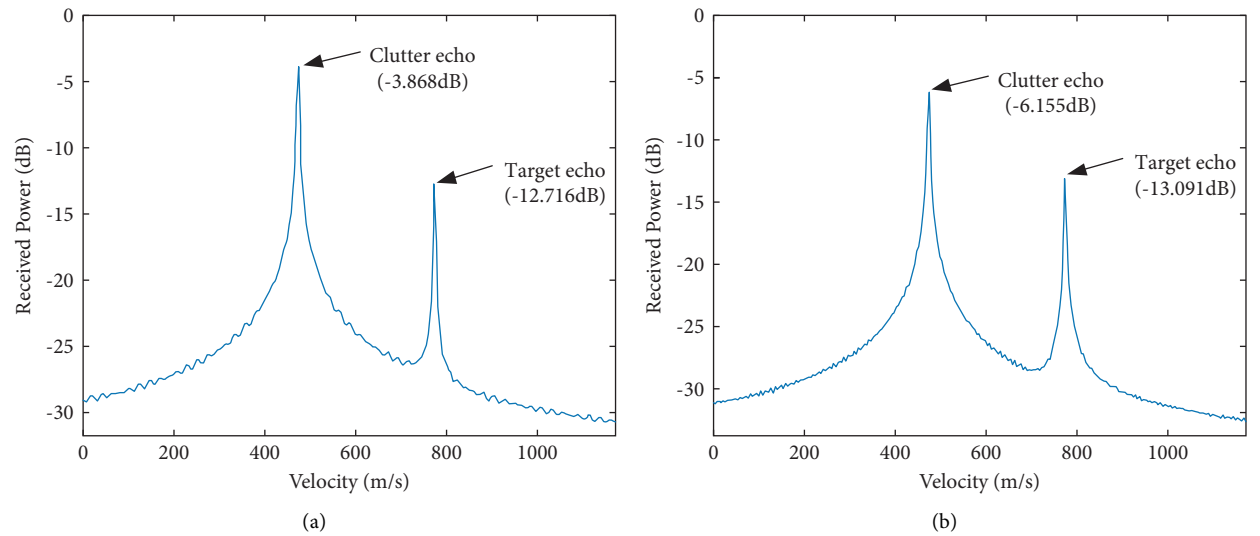

Figure 13: The echo power of target and clutter under different bandwidths (a) $B = 5$ M Hz; (b) 10 M Hz.

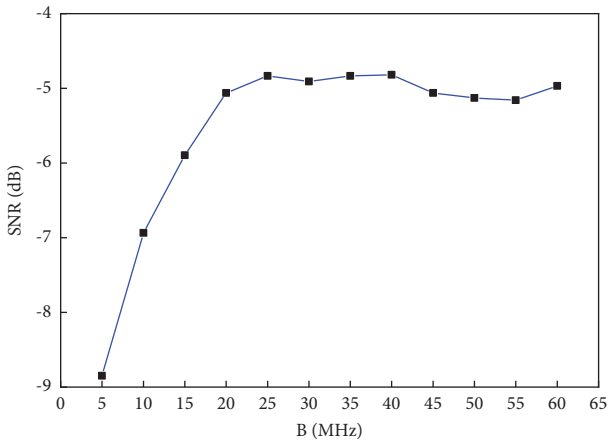

Figure 14: SNR under different signal bandwidths.

7. Conclusion

To better analyze the radar echo in a complex scene, this paper proposed a new radar echo simulation model for the ultra-low altitude targets. The model is based on the radar system and operating parameters. The calculation object is decomposed in space to obtain the equivalent scattering center unit. The time series of the transmitted signal is time-decomposed to obtain the time unit. The scattering information of the target and the environment is calculated by the modified four-path model and two-scale model. The echo signal of each unit is obtained by convolution of its scattering information with the time unit of the transmitted signal. Finally, the total echo signal is obtained by vector superposition.

In this paper, the electromagnetic scattering calculation and radar signal processing are innovatively integrated. The numerical simulation results show that the model in this paper can well separate the target signal from the sea clutter and multipath interference in the Doppler domain, which can intuitively display the target, multipath, and clutter information. The model in this paper can also be used to analyze the characteristics of a radar echo changing with various parameters, which has application value for target detection in a complex scene.

Data Availability

The data used to support the finding of this study are included in the article.

Conflicts of Interest

The authors declare that there are no conflicts of interest

Acknowledgments

This research was funded by the "National Natural Science Foundation of China," (grant number: 61901510) and "Natural Science Foundation of Shaanxi Province," (grant number: 2021 JQ-362).

References

[1] Y. Wang, X. Mao, and Z. Jie, "Effective sea clutter spectrum extraction method for HFSWR in adverse conditions," *Journal of Beijing Institute of Technology (Social Sciences Edition)*, vol. 22, no. 03, pp. 87–94, 2017.

[2] Y. Wang, L. I. Qun, and Y. Zhang, "A statistical distribution of quad-pol X-band sea clutter time series acquired at a grazing angle," *Acta Oceanologica Sinica*, vol. 37, no. 3, pp. 98–106, 2018.

[3] Z. Xin, G. Liao, Z. Yang, Y. Zhang, and H. Dang, "A deterministic sea-clutter space–time model based on physical sea surface," *IEEE Transactions on Geoscience and Remote Sensing*, vol. 54, no. 11, pp. 6659–6673, 2016.

[4] V. Karaev, Y. Titchenko, M. Panfilova, and E. Meshkov, "The Doppler spectrum of the microwave radar signal backscattered from the sea surface in terms of the modified bragg scattering model," *IEEE Transactions on Geoscience and Remote Sensing*, vol. 58, no. 1, pp. 193–202, 2020.

[5] P. B. Wei, M. Zhang, D. Nie, and Y. C. Jiao, "Statistical realisation of CWMFSM for scattering simulation of space-time varying sea surface," *International Journal of Remote Sensing*, vol. 40, no. 1, pp. 332–345, 2019.

[6] R. Sofiani, H. Heidar, and M. Kazerooni, "An efficient raw data simulation algorithm for large complex marine targets and extended sea clutter in spotlight SAR," *Microwave and Optical Technology Letters*, vol. 60, no. 5, pp. 1223–1230, 2018.

[7] D. A. G. Dell'Aglio, G. Di Martino, A. Iodice, D. Riccio, and G. Ruello, "A unified formulation of SAR raw signals from extended scenes for all acquisition modes with application to simulation," *IEEE Transactions on Geoscience and Remote Sensing*, vol. 56, no. 8, pp. 4956–4967, 2018.

[8] W. Jiang, L. Wang, and X. Li, "Simulation of a wideband radar echo of a target on a dynamic sea surface," *Remote Sensing*, vol. 13, 2021.

[9] T. Wang, C. Tong, and Y. J. Wang, "Radar echo simulation of ultra-low altitude target based on near-field scattering model," *Systems Engineering and Electronics*, vol. 44, no. 1, pp. 139–145, 2022.

[10] X. U. Zhiyong, "Subband synthesis method for simulation of wide band radar clutter," *IET International Radar Conference*, pp. 20–22, Guilin, China, 2009.

[11] W. B. Gordon, "High frequency approximations to the physical optics scattering integral," *IEEE Transactions on Antennas and Propagation*, vol. 42, no. 3, pp. 427–432, 1994.

[12] A. N. Nguyen and H. Shirai, "Electromagnetic wave scattering from dielectric bodies with equivalent current method," in *Proceedings of the 2013 International Conference on Electromagnetics in Advanced Applications (ICEAA)*, pp. 744–747, IEEE, Turin, Italy, September 2013.

[13] A. Arnold-Bos, A. Khenchaf, and A. Martin, "Bistatic radar imaging of the marine environment—Part I: theoretical background," *IEEE Transactions on Geoscience and Remote Sensing*, vol. 45, no. 11, pp. 3372–3383, 2007.

[14] A. Fung and K. Lee, "A semi-empirical sea-spectrum model for scattering coefficient estimation," *IEEE Journal of Oceanic Engineering*, vol. 7, no. 4, pp. 166–176, 1982.

[15] F. T. Ulaby, "Microwave remote sensing active and passive," *Rader remote sensing and surface scattering and emission theory*, vol. 36, pp. 848–902, 1982.

[16] J. T. Johnson, C. J. Baker, and G. E. Smith, "The monostatic-bistatic equivalence theorem and bistatic radar clutter," in *Proceedings of the IEEE European Radar Conference*, pp. 105–108, Rome, Italy, October 2014.

[17] T. Elfouhaily, B. Chapron, K. Katsaros, and D. Vandemark, "A unified directional spectrum for long and short wind-driven waves," *Journal of Geophysical Research: Oceans*, vol. 102, no. C7, pp. 15781–15796, 1997.

[18] A. G. Voronovich and V. U. Zavorotny, "Theoretical model for scattering of radar signals in K_u- and C-bands from a rough sea surface with breaking waves," *Waves in Random Media*, vol. 11, no. 3, pp. 247–269, 2001.

[19] D. C. Schleher, *MTI and Pulsed Doppler Radar*, Artech House, 1991.